

Prediction of stable insulating intermetallic compounds

M. Mihalkovič, M. Krajčí

Institute of Physics, Slovak Academy of Sciences, 84511 Bratislava, Slovakia

M. Widom

*Department of Physics, Carnegie Mellon University
Pittsburgh, PA 15213*

(Dated: August 13, 2018)

We explore the stability of structure exhibiting hybridization gaps across a broad range of binary and ternary intermetallic compositions by means of band structure and total energy calculations. This search reveals previously unknown metal-based insulators, some with large gaps exceeding 1 eV, such as Al_2Fe and Al_4IrRe . We confirm large gaps using a hybrid density functional including exact exchange, and predict a gap of 2.2 eV for AlMnSi in the Pearson type tP6 structure, which is a chemically ordered ternary variant of the prototype MoSi_2 (Pearson type tI6) structure.

PACS numbers:

I. INTRODUCTION

Certain intermetallic alloys are electrically insulating despite the good metallic characters of their constituent elements. A classic example of this is provided by the compound Al_2Ru which is insulating as result of gaps in its density of states around its Fermi level [1]. Such materials pose intriguing questions as to the origins of their insulating properties and additionally may find potential applications, for example as thermoelectric materials [2].

Previous studies [3–7] have explained the origins of this gap, and generalized the families of compounds in which it is expected to occur. The essential mechanism is to establish a gap between bonding and antibonding states through the creation and occupation of hybridized orbitals, then to exactly fill the bonding states. For structures based on the prototype MoSi_2 (Pearson type tI6) and TiSi_2 (Pearson type oF24) this occurs at composition $(\text{Al})_2(\text{Fe})$, where the parenthesis around (Al) indicates an aluminum-group metal of valence three (specifically Al or Ga) and (Fe) is an iron-group transition metal of valence eight (i.e. Fe, Ru or Os). Notice these choices result in a total of fourteen valence electrons per transition metal atom.

Gap width may be controlled by selection of the specific combinations of elements, or by alloying with adjacent elements in the periodic table (e.g. replacing the (Fe)-group element with a combination of (Mn)-group and (Co)-group), while maintaining constant valence per transition metal atom. Alternatively, we may replace half of the (Al)-group elements with (Si)-group, while simultaneously replacing the (Fe)-group transition metal with a (Mn)-group element.

Here we report a thorough study of the tI6 and oF24 alloy families. The crucial new feature of our work is we simultaneously evaluate the compounds' enthalpies of formation, so that we may predict cases where the proposed structures are likely to form as stable compounds, as bandgap engineering through chemical substitution requires monitoring both variation of band gaps as well as

thermodynamic stability relative to competing phase formation [8]. In this manner, we predict the occurrence of thirteen previously unknown compounds, each of which exhibit electronic band gaps. We then checked the gaps predicted by conventional DFT utilizing a hybrid functional including exact exchange. Among our newly predicted stable compounds is Al-Fe, with a gap of 1.1 eV, Al-Ir-Re, with a gap of 1.3 eV, and Al-Mn-Si with a gap of 2.2 eV.

II. STRUCTURES

Al_2Ru has been reported to occur in both the tI6 [9] and the oF24 [10] structures. Indeed, both structures share common structural elements, and are stabilized by similar mechanisms. The essential structural feature is an Ru-centered ring of six Al atoms (see Fig. 1), repeated periodically to tile the plane. A third structure, based on the CrSi_2 prototype (hP9) shares a similar motif. The ring is a slightly irregular hexagon, with only a 2-fold rotational symmetry. This ring lies perpendicular to the [110] axis in tI6 and the [001] axis in hP9 and oF24. The differences between structures rests in the stacking of these TM-centered rings (TM stands for transition metal). Consider a triangle of three TM atoms within a layer. There are four possible sites for the TM in an adjacent layer, either the vertex site or else one of the three edge centers of this triangle. In tI6 the TM alternates between two such sites, in hP9 between three and in oF24 all four sites are utilized.

Chemical ordering in ternary compounds lowers the symmetry from its binary prototype. For example, the MoSi_2 prototype is Pearson type tI6, space group $I4/mmm$, while the optimal decoration for AlMnSi is Pearson type tP6 (Primitive, not body centered) with space group $P4/nmm$. The chemical occupation is uniform within layers when the structure is viewed down the 4-fold axis. For example, an Al_2Mn layer alternates with an Si_2Mn layer (see Fig. 1b), rather than mixing Al

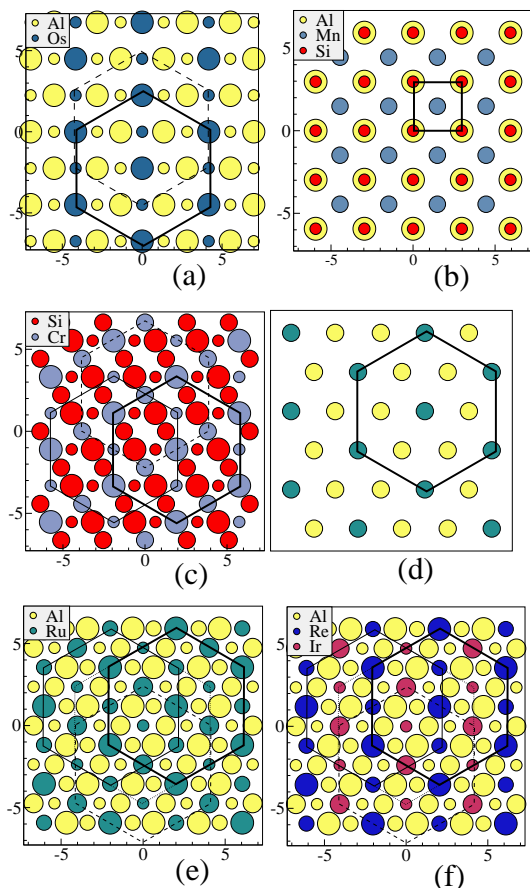


FIG. 1: Structures of the class. Colors indicate atomic species, size indicates vertical height. (a) Al_2Os in the Pearson tI6 (MoSi_2) structure. TM hexagons in alternate layers outlined in solid and dashed lines. (b) AlMnSi in tP6 structure. View along (001) axis reveals uniform chemical identity of layers, and relationship to cP2 (CsCl) structure. (c) CrSi_2 in the hP9 structure revealing three stacked hexagons. (d) Generic hexagon motif in single layer. (e) Al_2Ru in oF24 (Si_2Ti) structure reveals four stacked hexagon motifs. (f) Ternary decoration of Al_4IrRe in oF24 structure.

and Si within a layer. Likewise the Si_2Ti prototype of Pearson type oF24 has space group Fddd while the optimal decoration for AlIrRe maintains Pearson type oF24 but lowers the space group to F222 (Fig.1f). Energetically optimized Wyckoff positions for the two prototypical structures are given in Table I.

III. METHODS

We utilize VASP [11, 12] to carry out first principles total energy calculations. All atomic positions and lattice parameters are fully relaxed. We increase our k-point densities until energies have converged to 1 meV/atom. Default energy cutoffs are employed, which are sufficient to converge energy differences to this tolerance. Because of the volume relaxation, our energy may be considered

as an enthalpy at $P=0$ and $T=0\text{K}$. We adopt projector augmented wave potentials [13, 14], and for a density functional we choose the PBE generalized gradient approximation. Spin polarization is utilized in appropriate cases.

Conventional density functional theory generally underestimates band gaps, so we employ a hybrid functional [15], HSE06 [16], that includes a portion of exact exchange, to obtain more reliable values. However, the hybrid functional is computationally expensive so we do this only in selected cases. We also report pseudogap widths, which we define as the energy interval within which the density of states remains below 0.20 states/eV/atom.

Our stability calculations follow methods outlined in [17]. Primarily, we calculate enthalpy of formation ΔH by subtracting the calculated enthalpies from the enthalpies of the pure elements in their stable forms. In addition to the enthalpies of our tI6 and oF24 structures, we include all known structures within the given alloy system as well as selected hypothetical structures that occur in chemically similar systems.

In the case of ternary systems, the atomic decoration is not constrained, due to the mixing of TM species, or substituting (Si)-group for (Al)-group elements. To search for optimal patterns of chemical ordering, we first exhaustively enumerate all symmetry-independent configurations within cells specified below. We examine for two representative alloy systems of each class, to check for consistency of the optimal chemical decoration, and then subsequently apply the optimal decoration to all other ternary alloy systems from the corresponding family.

(B/C)Mn class. Our representative alloy systems were AlMnSi and AlReSi . In the MoSi_2 .tI6 prototype structure, we limited our ground state search to $1 \times 1 \times 2$ and $\sqrt{2} \times \sqrt{2} \times 1$ supercells. Each of these had 10 independent configurations. In the Si_2Ti .oF24 prototype case, the unit cell with 8 Si and 8 Al atoms occupying "Si" sites yields 293 independent configurations. We limited our ground-state search to configurations of relatively high symmetry.

Al(Mn/Co) class. Our representative alloy systems were AlIrRe and AlReRh . In the MoSi_2 .tI6 prototype structure, there are 2 independent configurations each in the $1 \times 1 \times 2$ and $\sqrt{2} \times \sqrt{2} \times 1$ supercells. In the Si_2Ti .oF24 prototype case, there were 8 independent assignments for transition metals on the "Ti" sites.

Given a database of relaxed structures, we calculate the convex hull of enthalpy as a function of composition. Predicted stable structures occupy the vertices of the convex hull. For structures that are *unstable*, we report the energy ΔE by which they lie above the convex hull. For stable compounds, negative values of ΔE indicate the formation enthalpy with respect to compounds of adjacent compositions.

Fig. 2 gives an example for the case of Al-Mn-Si. We reproduce the stability [18] of most known low temperature binaries, and two of the ternaries. One of these

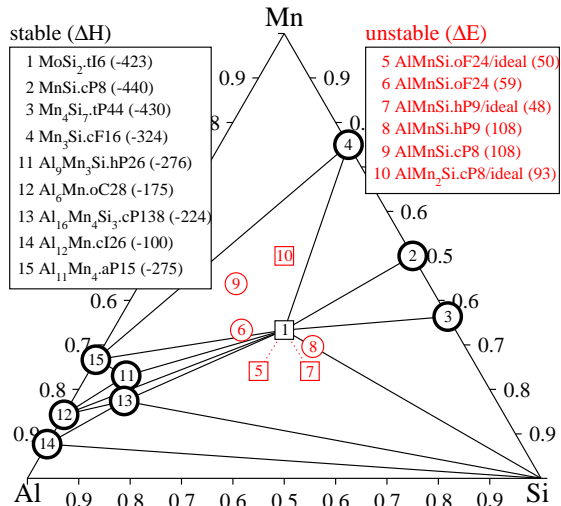


FIG. 2: (color online) Phase diagram of Al-Mn-Si. Heavy circles indicate known stable phases, light circles indicate known high temperature phases, squares indicate unknown structures or compositions. ΔH values are enthalpy of formation (meV/atom) of stable structures. Positive ΔE values are energies above the convex hull for unstable structures, while negative ΔE is the formation enthalpy with respect to adjacent compositions for stable structures.

Al	2c	0.75	0.75	0.9014	Ir	4a	0.0	0.0	0.0
Mn	2c	0.75	0.75	0.2736	Re	4d	0.75	0.75	0.75
Si	2c	0.75	0.75	0.5846	Al1	8f	0.50	0.6706	0.50
					Al2	8i	0.25	0.0817	0.25

TABLE I: Atomic structures of AlMnSi.tP6 (left block; space group P4/nmm (#129), $a=3.027\text{\AA}$, $c=7.932\text{\AA}$) and Al₄ReIr.oF24 (right block; group F222 (#22), $a=4.745\text{\AA}$, $b=8.139\text{\AA}$, $c=8.925\text{\AA}$). Wyckoff sites are labeled by site multiplicities.

ternaries (Al₁₆Mn₄Si₃.cP138) is an icosahedral quasicrystal approximant, and exhibits a gap in its density of states. However, two reported phases (Al_{0.6}Mn_{0.8}Si_{0.4} and Al₈Mn₃Si₉) have unknown structure and hence are omitted from our study, and three reported phases (Pearson types cP8, oF24 and hP9) exhibit partial site occupancy or mixed chemical occupancy and lie off their ideal stoichiometries, and hence are presumed to be stable only at high temperatures. Meanwhile, our predicted lowest energy of AlMnSi in the tP6 structure has not been reported experimentally. We suspect the prediction is correct, as the $\Delta E = -48$ meV/atom is well beyond the expected uncertainty of DFT, and our exact exchange calculation confirms stability of tP6. Perhaps oF24 is a high temperature phase whose entropy inhibits formation of the true low temperature tP6 phase through conventional sample preparation methods.

IV. RESULTS

Table II presents our predicted stable structures along with their band gaps (if any) and pseudogap widths. Complete data is given in Table II. We confirm the stability of Al₂Ru, Al₂Os, Ga₂Ru and Ga₂Os in the oF24 structure, and AlGeRe in the tI6 structure. We predict the stability of (Al,Ga)₄TcRh, (Al,Ga)₄ReIr and AlGeMn in the oF24 structure and Al₂Fe, AlSiMn, (Al,Ga)SiTc, GaSiRe, (Al,Ga)GeTc and GaGeRe in the tI6 structure.

We previously discussed the case of Al₂Fe [19]. Although total energy calculations predict it to be stable, the observed Al₂Fe phase is intrinsically disordered with low symmetry. This phase may be thermodynamically stabilized at high temperature by its vibrational entropy. It is probable that formation of the true low temperature stable phase is kinetically hindered at low temperatures. The most interesting new prediction may be AlMnSi, as it is comprised of common elements and it has the largest predicted true gap (2.2 eV, 1 eV larger than elemental silicon)

The electronic density of states and band structure of our predicted AlMnSi structure are shown in Fig. 3. As expected, the conventional DFT gap is severely underestimated, owing to the derivative discontinuity and delocalization error [20]. Inspecting the band structure, we see that the band gap is indirect. Projecting onto atomic orbitals we find the top of the valence band at Γ is purely d_{xy} localized on the Mn atoms, while the bottom of the conduction band, located along $\Gamma - X$ is a hybrid of Al and Si p_x and p_y with Mn d_{xz} and d_{yz} states. A nearly degenerate conduction band local minimum of similar hybridized character occurs along $M - \Gamma$. Another interesting feature is the nearly flat valence band minimum along $\Gamma - Z$, which is responsible for the step function-like onset of the density of states near $E = -15$.

V. DISCUSSION

We have predicted a large number of stable intermetallic compounds with hybridization gaps based on chemical ordering on underlying tI6 and oF24 structures, several of which have not been previously reported. In some cases they may not have been previously reported because the alloy systems have not been thoroughly evaluated. In the case of Al-Mn-Si, a chemically disordered phase of structure type oF24 is observed, while we identify the stable state as tP6 (a chemically ordered ternary variant of tI6). Presumably the entropy of chemical substitution and atomic vibrations stabilizes the disordered structure at high temperature, making identification of the low temperature stable structure difficult. Preliminary investigation confirms that both configurational and vibrational entropy of oF24 exceed that of tP6. While the oF24 structure also exhibits a gap, it is smaller than that of tP6, and the chemical disorder can be expected to

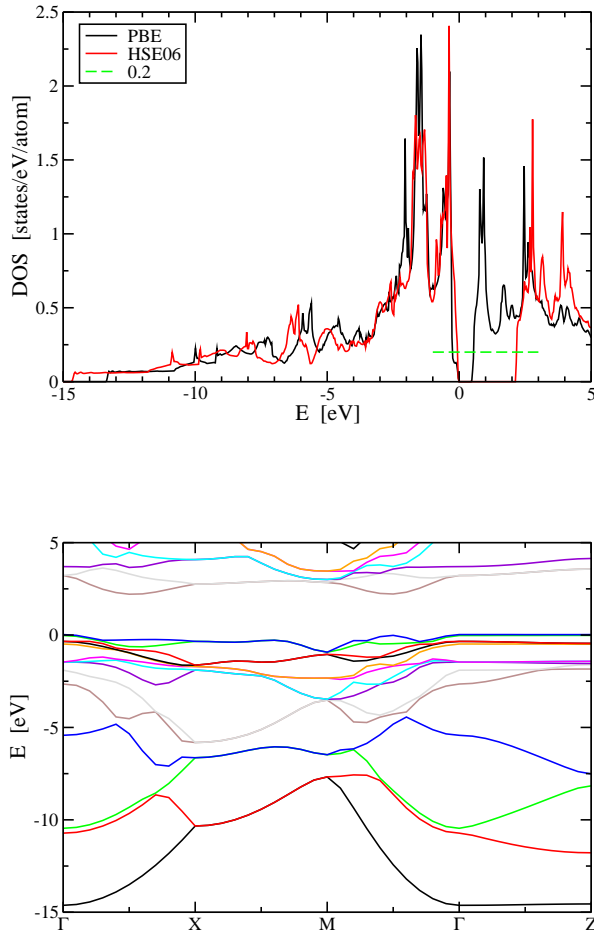


FIG. 3: (a) Electronic density of states of AlMnSi in the MoSi₂.tI6 structure. Shown are DOS for the PBE and HSE06 functionals with $E_F = 0$. Threshold of 0.2 states/eV/atom defines the pseudogap. (b) Band structure of AlMnSi in the MoSi₂.tI6 structure calculated using the HSE06 functional.

further diminish the gap in this high temperature phase. Thus, experimental efforts to identify the true low temperature stable phase are especially welcome.

Acknowledgments

MM and MK were supported by Slovak Research and Development Agency grants APVV-0647-10, APVV-0076-11 and VEGA 2/0111/11.

-
- [1] D. Manh, G. de Laissardiere, J. Julien, D. Mayou, and F. Cyrot-Lackmann, *Solid State Communications* **82**, 329 (1992)
- [2] T. Takeuchi, Y. Toyama, A. Yamamoto, H. Hazama, and R. Asahi, *Mat. Trans.* **51**, 1127 (2010)
- [3] M. Weinert and R. E. Watson, *Phys. Rev. B* **58**, 9732 (1998)
- [4] M. Krajci and J. Hafner, *Journal of Physics: Condensed Matter* **14**, 5755 (2002)
- [5] M. Krajci and J. Hafner, *Journal of Physics: Condensed Matter* **14**, 7201 (2002)
- [6] D. C. Fredrickson, S. Lee, R. Hoffmann, and J. Lin, *Inorg. Chem.* **43**, 6151 (2004)
- [7] D. C. Fredrickson, S. Lee, R. Hoffmann, and J. Lin, *Inorg. Chem.* **43**, 6159 (2004)
- [8] R. Sun and G. Ceder, *Phys. Rev. B* **84**, 245211 (Dec 2011)
- [9] W. Obrowski, *Metall (Heidelberg)* **17**, 108 (1963)
- [10] L. E. Edshammar, *Acta Chem. Scand.* **20**, 427 (1966)
- [11] G. Kresse and J. Hafner, *Phys. Rev. B* **47**, RC558 (1993)
- [12] G. Kresse and J. Furthmuller, *Phys. Rev. B* **54**, 11169 (1996)
- [13] P. E. Blochl, *Phys. Rev. B* **50**, 17953 (1994)
- [14] G. Kresse and D. Joubert, *Phys. Rev. B* **59**, 1758 (1999)
- [15] J. Paier, R. Hirschl, M. Marsman, and G. Kresse, *J. Chem. Phys.* **122**, 234102 (2005)
- [16] J. Heyd, G. E. Scuseria, and M. Ernzerhof, *J. Chem. Phys.* **124**, 219906 (2006)
- [17] M. Mihalkovič and M. Widom, *Phys. Rev. B* **70**, 144107 (2004)

- [18] A. Prince, in *ASM Alloy Phase Diagram Center*, edited by P. Villars (ASM International, OH, 1993) <http://www1.asminternational.org/AsmEnterprise/APD>
- [19] M. Mihalkovič and M. Widom, *Phys. Rev. B* **85**, 014113 (Jan 2012)
- [20] M. K. Y. Chan and G. Ceder, *Phys. Rev. Lett.* **105**, 196403 (Nov 2010)

Al ₂ (Fe)		PBE		HSE06		Ga ₂ (Fe)		PBE		HSE06					
Chem	Struct	ΔE	ΔH	E_g	E_p	E_g	E_p	Chem	Struct	ΔE	ΔH	E_g	E_p	E_g	E_p
Al-Fe	<i>Ortho</i>	22	-335	0.220	0.650	0.739	1.287	Ga-Fe	<i>Ortho</i>	127	-94	0.141	0.469	0.614	1.115
	Tetra	-21	-358	0.008	0.401	1.115	1.663		<i>Tetra</i>	182	-39	0.011	0.016	0.001	0.016
Al-Ru	<i>Ortho</i>	-17	-685	0.112	1.119	0.591	1.669	Ga-Ru	<i>Ortho</i>	-20	-377	0.107	0.928	0.559	1.448
	<i>Tetra</i>	33	-653	0.005	0.556	0.489	1.319		<i>Tetra</i>	74	-303	0.014	0.527	0.274	1.149
Al-Os	<i>Ortho</i>	-0.7	-560	0.698	1.287	1.061	2.060	Ga-Os	<i>Ortho</i>	76	-156	0.644	1.142	1.199	1.767
	<i>Tetra</i>	0.7	-559	0.354	1.151	1.057	1.882		<i>Tetra</i>	107	-125	0.008	0.987	0.669	1.752
Al ₄ (Mn)(Co)		PBE		HSE06		Ga ₄ (Mn)(Co)		PBE		HSE06					
Chem	Struct	ΔE	ΔH	E_g	E_p	E_g	E_p	Chem	Struct	ΔE	ΔH	E_g	E_p	E_g	E_p
Al-CoMn	<i>Ortho</i>	43	-364	0.274	0.700	0.690	1.413	Ga-CoMn	<i>Ortho</i>	93	-144	0.277	0.554	x	x
	<i>Tetra</i>	39	-368	0.028	0.394	0.605	1.545		<i>Tetra</i>	163	-74	0.014	0.241	x	x
Al-TcRh	Ortho	-50	-693	0.425	1.125	x	x	Ga-TcRh	Ortho	-76	-402	0.307	1.024	0.805	1.666
	<i>Tetra</i>	50	-643	0.013	0.528	0.023	1.199		<i>Tetra</i>	76	-326	0.014	0.429	x	x
Al-ReIr	Ortho	-40	-597	0.702	1.326	1.260	1.999	Ga-ReIr	Ortho	-18	-234	0.905	1.250	1.426	1.833
	<i>Tetra</i>	85	-513	0.000	0.009	0.001	0.522		<i>Tetra</i>	57	-177	0.009	0.751	x	x
Al(Si)(Mn)		PBE		HSE06		Ga(Si)(Mn)		PBE		HSE06					
Chem	Struct	ΔE	ΔH	E_g	E_p	E_g	E_p	Chem	Struct	ΔE	ΔH	E_g	E_p	E_g	E_p
AlSi-Mn	<i>Ortho</i>	50	-356	0.48	0.84	1.195	1.353	GaSi-Mn	<i>Ortho</i>	134	-169	0.599	0.614	x	x
	Tetra	-48	-403.0	0.435	0.821	2.156	2.254		<i>Tetra</i>	54	-249	0.370	0.681	1.761	2.022
AlSi-Tc	<i>Ortho</i>	76	-528	1.101	1.174	1.757	1.829	GaSi-Tc	<i>Ortho</i>	30	-382	0.925	1.025	x	x
	Tetra	-76	-604	0.485	1.351	1.320	2.498		Tetra	-30	-412	0.363	1.194	1.181	2.223
AlSi-Re	<i>Ortho</i>	72	-395	0.336	0.954	1.050	1.614	GaSi-Re	<i>Ortho</i>	132	-164	0.323	0.856	0.902	1.483
	<i>Tetra</i>	-33	-467	0.277	1.615	0.862	2.637		Tetra	-54	-296	0.135	1.230	0.908	2.295
AlGe-Mn	Ortho	-20	-164	0.612	0.645	0.000	0.000	GaGe-Mn	<i>Ortho</i>	90	26	0.504	0.541	x	x
	<i>Tetra</i>	20	-144	0.478	0.638	x	x		<i>Tetra</i>	68	3	0.212	0.489	x	x
AlGe-Tc	<i>Ortho</i>	21	-402	0.754	0.953	x	x	GaGe-Tc	<i>Ortho</i>	19	-216	0.694	0.872	x	x
	Tetra	-21	-423	0.311	1.089	1.151	2.107		Tetra	-19	-235	0.178	0.869	0.880	1.816
AlGe-Re	<i>Ortho</i>	63	-178	0.172	0.781	x	x	GaGe-Re	<i>Ortho</i>	71	40	0.199	0.745	x	x
	<i>Tetra</i>	-43	-241	0.106	1.415	0.870	2.284		Tetra	-20	-30	0.019	0.861	0.811	1.907

TABLE II: Stability and bandgap data for various alloy systems. Element names in parenthesis indicate columns of the periodic table. ΔH and ΔE are enthalpy of formation and instability energy in units of meV/atom. E_g and E_p are the energy gap and pseudogap in units of eV. PBE and HSE06 are the density functionals. Newly predicted stable structures are in bold. Previously known and reconfirmed stable structures are in italics. Maximum gap and pseudogap are in bold.